A HYBRID SEQUENTIAL SCHEME FOR BRITTLE HYDRAULIC FRACTURES IN POROELASTIC MEDIA

J.M.M. LUZ FILHO, M. XAVIER, M.A. MURAD AND A.A. NOVOTNY

Abstract. We construct a new operator splitting scheme to describe a fluid-driven brittle fracture propagation in a Biot medium based on a time-scale separation assumption. In this context, we propose an alternate hybrid time-stepping scheme where in the injection step, prior to fracture advance, we explore the framework of the fixed stress split scheme with hydrodynamic subsystem solved ahead of the geomechanics for a frozen total mean stress. Conversely after convergence of the fixed stress split iterations, when the pore pressure exceeds a critical value, the coupling between poromechanics and fracture propagation is accomplished by considering a fast time-scale, with frozen pore-pressure and Darcy velocity fields. Such a latter step is performed in a separate iteration loop with the elasticity sub-system incorporating the Francfort-Marigo variational model for a thin damage region. In this setting, the evolution of the damaged zone is governed by the sensitivity of the associated shape functional with respect to the nucleation of a small damaged zone, which is computed within the framework of the topological derivative method. The resulting approach is algorithmically described in details. A numerical assessment of the model is constructed by performing a series of benchmark examples, showing different features of the proposed approach such as characterization of fracture-activation pressure, crack path forecast, and the ability to capture kinking and bifurcations and quantifying the effects of the *in situ* stress field on the crack path.

1. Introduction

Hydraulic fracturing is a process largely applied by oil and gas industries. Such a well stimulating-based technique, also commonly referred to as *fracking*, was first proposed in [14] and consists in increasing the production area along with enhancing the permeability of the geological formation. The induced fracture network is typically generated by pumping an aqueous phase with controlled composition at high pressure through a pressurized wellbore [11]. Furthermore, in order to extend the size of the propagation region, substantial pressure increase is required in order to overcome the porous medium resistance along with the *in situ* stress state in the rock layers above the well. The main drawbacks of the technique are related to environmental impacts associated with hydrocarbon leakage to adjacent water resources and possible trigger of induced seismicity. Nevertheless, in spite of the above issues, from the economical point of view, fracking has been considered one of the most viable techniques commonly adopted to enhance hydrocarbon recovery. Among other aspects, such environmental and economical issues reinforce the need for detailed studies on this subject, particularly the necessity of developing robust and accurate computational models with the ability to monitor, optimize and improve our knowledge on the mechanics underlying the process in order to perform it safely.

1.1. **The hydraulic fracturing modeling.** The construction of models to describe hydraulic fracturing has been subject of many studies over the last years, see for instance [8, 21, 35, 37, 43]. To date, since the forerunner Griffith theory of linear elastic fracture mechanics, crack propagation has been extensively studied with different approaches, (see

Date: January 9, 2022.

Key words and phrases. Brittle hydraulic fractures, fixed-stress-split, poroelasticy, Francfort-Marigo damage model, topological derivative method.

[16] for an exhaustive review) where we may distinguish two different schools of thought, one based on discontinuous models whereas the other is hinged upon continuous models. The first comprises the well-known discontinuous (discrete-type) models, where we may highlight Barenblatt's Cohesive Zone Model [4] and the enriched-based finite element methods, such as XFEM, wherein the displacement discontinuities are captured by the design of richer approximation spaces [26]. In this setting, the advance of the discontinuity is tracked explicitly by updating the enriched basis functions. On the other hand, the latter group of theories hinges upon continuous, or smeared out, diffusive-based approaches based on minimization of the total energy of a cracked solid. Such a family of smeared out type-approaches avoids the need of enrichment and constant updates of finite element basis functions, allowing the use of standard Galerkin methods in the discretization of the system flow and mechanics stemming from the fixed stress split scheme. In this setting, among the proposed continuum damage theories, we may highlight the functional-based approach constructed by Francfort and Marigo [17, 18], who also developed the proper mathematical framework for the underlying variational method. Two popular models lying in this category are the phase field fracture model [12, 13] and topological derivative based approaches [41, 42]. Phase field fracture models (PFF), hinging upon the regularisation procedure proposed in [7], were inspired by Ambrosio and Tortorelli [3] in the context of elliptic perturbation of the free-discontinuity problem, which commonly appears in image segmentation problems [27]. When applied to crack propagation, PFF-models rely upon the regularised version of Griffith's isotropic brittle fracture problem based on the minimization approach of a total energy, given by the sum of a stored elastic component and the dissipated surface energy associated with the crack, which is envisioned as a lower $(d-1)$-dimensional hyper-surface. In spite of its versatility in modeling a wide diversity of fracture networks, along with the capability of handling topologically complex geometries, owing to the lack of coercivity of the corresponding shape functional, the discontinuity in PFF-models requires the characterization of a regularization length scale, so that the sharp crack is smeared over a localization band, described by the so-called crack phase field parameter. Thus, PFF-model is typically regarded as an approximation of the Francfort and Marigo's variational approach to fracture in the vanishing limit of the regularization parameter. Despite the underlying damage mechanism, the constitutive laws of PFF-models exhibit crucial differences compared to those of continuum damage models (CDM). As shown in [23], the evolution law for the grow of the damaged zone is not embedded in the classical continuum damage models, but rather, incorporated in the evolution of the phase-field parameter in the perturbed Euler-Lagrange equations.

1.2. **Hydraulic fracturing variational approach.** The variational approach of Francfort and Marigo combined with the phase-field regularised formulation do not consist of the unique approximation methodology. Alternative methods seated on the topological derivative concept, which quantifies the sensitivity of the elastic-damage functional with respect to an infinitesimal singular domain perturbation, have drawn increasingly attention to tackle fracture propagation problems characterized by the evolution of sharp interfaces dividing healthy and fully damaged zones [1, 39, 40]. In addition to the underlying physical nature of the Francfort–Marigo variational functional based on damage mechanisms, the approach has also shown great ability to capture crack propagation with high accuracy. More specifically, the framework of topology optimization combined with sharp-damage based models has shown great capability and remarkable flexibility in modeling numerically the evolution of abrupt interfaces [1, 39, 40]. In this context, rather than adopting elliptic regularization, the derivative of the shape functional with respect to perturbations in the non-damaged phase can be computed within the framework of a gradient descent method and combined with a level set-type method. It is remarkable

to observe that in this alternative context, unlike the empirical damage formulations, the evolution of the damage front is consistently advected in the direction of the (minus) shape functional gradient, which can be precisely quantified by the topological derivative.

The Francfort-Marigo variational formulation has been successfully explored within the aforementioned methods giving rise to a wide range of different frameworks, such as the ones based on level-set [1], phase-field [7] and topological derivative [40] approaches. In particular, the topological derivative method consists of a natural tool to deal with fracture mechanics modeling. Within this framework applied to fracking, Xavier et al. [42] considered a forward poroelastic model with a stress-free reference state governed by a semi-coupled flow/geomechanics system, with the hydrodynamics treated as a sequence of stationary states. In spite of these time-scale assumptions, the approach proposed in [42] allows for dealing with multiple crack tips and detecting numerous crack paths simultaneously. Moreover, it has shown flexibility in capturing the activation pressure along with incorporating phenomena such as kinking and bifurcations in the discrete network.

1.3. **A hybrid sequential scheme for hydraulic fracturing.** In this work we aim at extending the methodology developed in [42] to the fully transient poroelastic forward problem adopting the framework of sequential schemes applied to Biot's poroelasticity model. Since the seminal papers [5, 6] for soil consolidation, coupled hydro-mechanical effects have been described by the so-called fully coupled formulations where mechanics and hydrodynamics are solved simultaneously [29]. Despite its prominence, particularly for consolidation [24], fully-coupled models exhibit several drawbacks. Among them we may highlight the compatibility between the finite element spaces for pressure and displacements in order to fulfill stability requirements, particularly in the nearly incompressible (undrained) conditions [28, 29, 30, 34], which may incur the appearance of oscillations in the pore pressure field. Moreover, the discretization of the fully-coupled formulation sometimes leads to the resolution of unpractical systems with a large number of degrees of freedom, imposing huge computational costs, highly challenging code management, along with precluding the use of different time steps for flow and mechanics. To remedy these deficiencies, a family of sequential coupling algorithms has been recently devised, which consists of a trustworthy approach. Within this alternative context, several schemes seated on operator splitting methods have been constructed which pursue the partitioning of the global system into sub-problems with coupling enforced in an iterative fashion. Without attempting to be exhaustive, we refer to [15, 36, 38]. In this general context, different formulations have been constructed, where we may highlight the fixed drained and undrained splits, where the geomechanics subsystem is solved ahead of the flow. The former is conditionally stable whereas the accuracy of the latter deteriorates substantially with the grow of the undrained Biot modulus in the nearly incompressible limit [22]. Among the schemes where hydrodynamics is solved first, we may highlight the fixed strain and stress splits. The former behaves conditionally stable whereas the unconditional stable fixed stress split is far more efficient, since the source term involving the time-derivative of the total mean stress admits a much slower characteristic time scale compared to the other poromechanical variables. Among the wide diversity of sequential schemes, the unconditional stable fixed stress split, based on freezing the total mean stress in the flow equations, has shown enormous efficiency and unconditional stability [2, 20, 22, 25], and is now recognized as a potential sequential algorithm for coupling flow and geomechanics. In the above context, it is worth mentioning the underlying implicit nature of the fixed stress split which does not suffer from the drawbacks of explicit schemes.

The purpose of this work is to explore the Francfort-Marigo framework under a different perspective, by proposing an alternative computational model to describe crack propagation in brittle poroelastic media, seated on a continuum damage theory with abrupt interfaces, also exploring the good features of the fixed stress split scheme. In this new context, the associated shape functional for modeling the damage evolution phenomenon is minimized with the help of the topological derivative method. The synergy between the above ingredients, all together, allows to construct an innovative description of crack propagation in poroelastic media. In contrast to PFF-type approaches, an essential feature underlying the computational model proposed herein is the avoidance of the necessity of introducing additional regularized unknowns in the poroelastic model, as the theory attributes two distinct values for the poroelastic coefficients, each one corresponding to the healthy/damaged sub-domains. Our aim is two-fold. As a first goal, the Francfort-Marigo shape functional is minimized with the help of the topological derivative method, where we proceed beyond the quasi-steady approach proposed in [42], in the context of transient fixed stress representation of the poroelasticity system. In addition to the well-known time-scale assumption underlying the fixed stress split scheme, the target description of crack propagation, addressed in the subsequent stage to the fixed stress split scheme, entails the characterization of a secondary time-scale which dictates the evolution of poroelastic variables during fracking. For brittle geomaterials, we explore the separation between the characteristic time-scales underlying fracture evolution and fluid percolation, by postulating a frozen pore pressure field during crack propagation. Based on this key assumption, we can construct a hybrid time-evolution scheme for the forward and optimization sub-systems. In addition, the topological derivative formula associated with the quasi-static scenario derived [42] can be promptly adapted to the current transient context. Our second goal relies on exploring the effects of *in situ* stress profiles upon the crack propagation patterns. Within the variational statement of the fixed stress split version of the poroelasticity system such a contribution appears as an additional component in the linear functional in the right-hand side of the weak form. Different contrasts between vertical and horizontal *in-situ* stresses are analysed and shown to have a profound impact on the numerical crack patterns.

1.4. **Paper organization.** The resulting framework is algorithmically presented in details and substantiated with a set of numerical experiments. The discrete-in-time formulation relies strongly on the aforementioned time-scale assumption and shall be referenced herein to as *hybrid formulation*, where the flow subsystem of the fixed stress split problem is solved within the usual freezing of the total mean stress in the time-increments prior to fracking. In contrast, in the iterative process seated on the topological derivative for describing crack propagation, the flow subsystem remains frozen and only the material properties of the elastic subsystem are updated based on the topological derivative. To illustrate the performance of the proposed approach, a series of benchmark examples is presented showing different features of the formulation such as characterization of activation pressure, crack path forecast including kinking and bifurcations as well as effect of *in situ* stress upon the crack path. The framework proposed herein can be summarized as follows:

(1) At a new time step, run the fixed stress split algorithm for solving the hydromechanical system;
(2) After convergence, evaluate the topological derivative and check for the crack propagation criterion;
   (a) If the criterion is fulfilled, increase the damaged region according to the topological derivative, solve the geomechanical subsystem and go to (2);
   (b) Otherwise, return to (1);

In particular, the work is organized as follows. In Section 2, the hydro-mechanical model of fracking is introduced. In Section 3, the associated topological derivative is adapted from the quasi-static case derived in [42]. The topology optimization algorithm is presented in Section 4. The numerical experiments are driven in Section 5. Finally, some concluding remarks are presented in Section 6.

2. A sequential formulation for crack propagation in poroelastic media

In the subsequent developments, we present the steps underlying the new sequential two-stage methodology seated on an operator splitting scheme for describing propagation of a brittle crack in a Biot medium.

2.1. **A fixed stress split scheme for the sharp damage problem.** We begin by stating the extended poroelastic formulation to describe localized sharp damage between two distinct subdomains due to the presence of a crack. In the context of sequential coupling for flow and mechanics subsystems, the Biot model is rephrased within the framework of the fixed stress split scheme (see [25] for details). Thus, consider an open and bounded geometric domain $\Omega \subset \mathbb{R}^d (d = 2, 3)$ representing a poroelastic medium with strong localized contrast in the poromechanical properties in the vicinity of the crack. Within the current setting of sharp damage brittle behavior, the domain Ω contains a subdomain ω occupied by a preexisting fracture with degrading properties. Denoting t the characteristic time $(0 < t < T)$, within the context of the fixed stress split scheme, we seek the rock displacement $u(x, t)$ and pore pressure $p(x, t)$ fields satisfying [20]

$$\begin{cases} \operatorname{div}(\sigma(u)) = \alpha \nabla p - \operatorname{div}(\sigma_0) & \text{in } \Omega \times (0, T)\,, \\ \beta^* \partial_t p - \operatorname{div}(k \nabla p) = -\dfrac{\alpha}{K} \partial_t \overline{\sigma}_{\text{tot}} & \text{in } \Omega \times (0, T)\,, \end{cases} \tag{2.1}$$

endowed with appropriate initial and boundary conditions. In (2.1), $\overline{\sigma}_{\text{tot}}$ denotes the total mean stress, σ_0 and $\sigma(u)$ the *in-situ* (prior to fracking) and time-dependent components of the effective stress tensor, whereas k, K, α and β^* designate the hydraulic conductivity tensor, bulk modulus of the rock matrix, the Biot-Wilis coefficient and overall compressibility of the solid/fluid mixture, respectively. By denoting $\mathbb{C}$ the elastic tensor of the matrix and $\{K_S, K_F, \phi_L\}$ the undrained and fluid bulk moduli and the Lagrangian porosity, for an isotropic rock skeleton, the hydraulic conductivity k reduces to a scalar and the tensor $\mathbb{C}$ can be represented by the pair of Lamé coefficient $\{\lambda, \mu\}$ in the form $\mathbb{C} = 2\mu\mathbb{I} + \lambda(\mathrm{I} \otimes \mathrm{I})$, where $\mathbb{I}$ and I are the fourth and second order identity tensors, respectively. Therefore, we have the reduced constitutive laws

$$\sigma(u) = \lambda \operatorname{div}(u)\mathrm{I} + 2\mu\varepsilon(u), \quad \text{with} \quad \varepsilon(u) = \frac{1}{2}(\nabla u + \nabla u^\top), \tag{2.2}$$

and

$$\alpha = 1 - \frac{K}{K_S} \quad \text{and} \quad \beta^* = \left(\frac{1}{M} + \frac{\alpha^2}{K}\right), \quad \text{with} \quad \frac{1}{M} = \frac{\alpha - \phi_L}{K_S} + \frac{\phi_L}{K_F}, \tag{2.3}$$

where M represents the Biot's modulus and

$$\mu = \frac{E}{2(1+\nu)} \quad \text{and} \quad \lambda = \frac{\nu E}{(1+\nu)(1-2\nu)}\,, \tag{2.4}$$

with E and ν the Young modulus and the Poisson ratio of the rock skeleton, respectively. Finally, the total mean stress $\overline{\sigma}_{\text{tot}}$ is given by

$$\overline{\sigma}_{\text{tot}} = \overline{\sigma}_0 + K \operatorname{div}(u) - \alpha p\,, \quad \text{with} \quad \overline{\sigma}_0 = \frac{1}{3}\operatorname{tr}(\sigma_0)\,. \tag{2.5}$$

It is worth noting that owing to the avoidance of including intrusively regularised unknowns in the field-equations, the above formulation preserves the traditional structure of the poroelastic model. On the other hand, one has to keep track of the highly localized discontinuity property underlying the set of coefficients $\{\lambda, \mu, \alpha, k, \beta^*\}$. More precisely, since the domain Ω contains the subdomain ω representing the damaged zone, the parameters assume distinct values in the matrix $\Omega\backslash\overline{\omega}$ and fracture ω, giving rise to localized jumps in their magnitude across the sharp interface $\partial\omega$.

2.2. **Crack propagation based on damage with abrupt interface.** We now proceed by presenting the damage model which will be subsequently explored in the second stage of the operator splitting methodology. To this end, we begin by introducing an indicator-like function ρ in the form

$$\rho = \rho(x) := \begin{cases} 1, & \text{if } x \in \Omega\backslash\overline{\omega}\,, \\ \rho_0, & \text{if } x \in \omega\,, \end{cases} \tag{2.6}$$

with $0 < \rho_0 \ll 1$. The two-value image of the indicator function characterizes the region $\Omega\backslash\overline{\omega}$ as the healthy (undamaged) medium, whereas ω represents the degrading sub-portion occupied by the crack (Figure 1). Such an abrupt damage behavior is described by the traditional heterogeneous constitutive law for the effective stress tensor $\sigma(u) = \rho(x)\mathbb{C}\varepsilon(u)$.

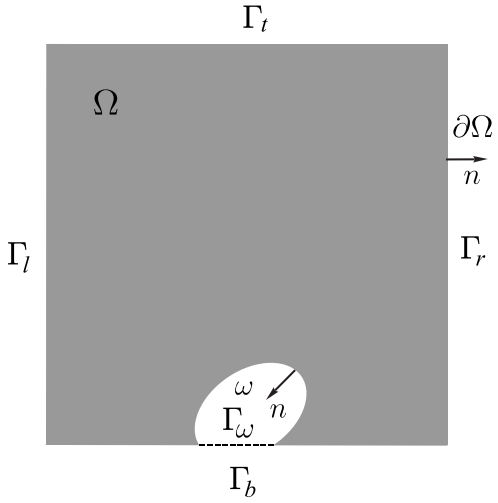

FIGURE 1. Geological block containing a pre-existing crack. The outer boundary is decomposed in disjoint subsets $\partial\Omega = \Gamma_b \cup \Gamma_r \cup \Gamma_t \cup \Gamma_l$.

In the sequel, we attach the Francfort-Marigo damage model to the evolution of the degrading region. Such an approach hinges upon the minimization of the shape functional $\mathcal{F}_\omega(u, p)$

$$\mathcal{F}_\omega(u, p) = \mathcal{J}(u, p) + \kappa|\omega|\,, \tag{2.7}$$

with respect to perturbations in the topology of the crack region ω. In (2.7), $\kappa|\omega|$ is the Griffith's energetic dissipation term with the symbol $|\cdot|$ used to denote the Lebesgue measure of the damaged phase ω. The parameter κ represents a material property that quantifies the resistance to damage. Such a parameter satisfies the bound [18]

$$\kappa < \frac{1-\rho_0}{2}\mathbb{C}\varepsilon(u)\cdot\varepsilon(u)\,. \tag{2.8}$$

In addition, $\mathcal{J}(u, p)$, defined as

$$\mathcal{J}(u, p) = \frac{1}{2}\int_\Omega \sigma(u)\cdot\varepsilon(u) - \int_\Omega \alpha p\ \mathrm{div}(u) + \int_\Omega \sigma_0\cdot\varepsilon(u)\,, \tag{2.9}$$

designates the total potential energy of the poroelastic system. It is worth pointing out that from (2.7), the Francfort-Marigo functional incorporates the geomechanical component of a typical Biot medium supplemented by a dissipation term associated with crack propagation. For application of the methodology based on the topological derivative, we refer to the canonical picture depicted in Figure 1. In this setting, we consider a geological block subject to tractions induced by the *in-situ* stress on the top boundary Γ_t, along with symmetry conditions on the left Γ_l and right Γ_r sides, aiming at mimicking the interactions with the adjacent blocks; as well as clamped condition on the bottom Γ_b. We also consider absence of normal flux on both $\Gamma_l \cup \Gamma_r$ and $\Gamma_b \setminus \Gamma_\omega$ together with reference pressure and well (injection) pressure prescribed on Γ_t and Γ_ω, respectively.

In what follows, we present the weak form of the flow and mechanics subsystems. To this end, in light of the boundary conditions described above, we introduce the appropriate functional spaces. For the mechanical sub-system, let the spaces $\mathcal{U}$ and $\mathcal{V}$ defined as

$$\mathcal{V} = \mathcal{U} := \{\varphi \in H^1(\Omega;\mathbb{R}^2) : \varphi_{|\Gamma_b} = 0,\ \varphi \cdot n_{|\Gamma_r \cup \Gamma_l} = 0\}\,, \tag{2.10}$$

whereas for the flow problem introduce the set $\mathcal{P}$ and the space $\mathcal{Q}$ in the form

$$\mathcal{P} := \{\phi \in H^1(\Omega) : \phi_{|\Gamma_t} = \overline{p}_0,\ \phi_{|\Gamma_\omega} = \overline{p}\}\,, \tag{2.11}$$

with $\overline{p}_0$ and $\overline{p}$ the reference (initial), and injection pressures, respectively and

$$\mathcal{Q} := \{\phi \in H^1(\Omega) : \phi_{|\Gamma_t} = 0,\ \phi_{|\Gamma_\omega} = 0\}\,. \tag{2.12}$$

We then have to find $u \in \mathcal{U}$, such that

$$\int_\Omega \sigma(u) \cdot \varepsilon(v) = \int_\Omega \alpha p\, \mathrm{div}(v) - \int_\Omega \sigma_0 \cdot \varepsilon(v)\,, \quad \forall v \in \mathcal{V}\,. \tag{2.13}$$

In addition, for the hydrodynamics we seek $p \in \mathcal{P}$, such that

$$\int_\Omega \beta^* \partial_t p\ q + \int_\Omega k \nabla p \cdot \nabla q = -\int_\Omega \frac{\alpha}{K} \partial_t \overline{\sigma}_{\mathrm{tot}}\ q\,, \quad \forall q \in \mathcal{Q}\,. \tag{2.14}$$

Considering the initial condition $p(x,0) = \overline{p}_0$, the function $\overline{p} = \overline{p}(t)$ represents the path in the time domain associated with the prescribed pressure on Γ_ω. For the sake of simplicity, we consider linear grow in the form

$$\overline{p}(t) := \begin{cases} \overline{p}_0 + rt, & 0 < t < t^*\,, \\ \overline{p}^*, & t^* \leq t < T\,, \end{cases} \tag{2.15}$$

with $\overline{p}_0$ the reference pressure at $t = 0$ and r the increment pressure rate over Γ_ω. In addition, t^* designates the characteristic time of the injection and $\overline{p}^*$ the maximum well pressure.

Hence, following the Francfort-Marigo model of sharp interface damage, for a frozen in time pore pressure field $p_c(x) = p(x,t_c)$, crack propagation is governed by the following minimization problem

$$\underset{\omega \subset \Omega}{\mathrm{Minimize}}\ \mathcal{F}_\omega(u,p_c),\ \text{subject to (2.13)}\,, \tag{2.16}$$

where p_c is the critical pressure in which the fracture starts to grow at the critical time t_c. Here, we shall refer to as the critical pressure of activation, the value of pressure on Γ_ω capable of triggering crack propagation.

An inherent difficulty of problems with stress singularities based on the Francfort-Marigo model is that the strain energy density rises locally to unbounded values at the crack tip, and thus above any finite threshold. In this sense, following the strategy proposed in [41, 42] regarding the characterization of the critical pressure of crack activation

p_c, the parameter κ is replaced by κ_δ defined as

$$\kappa = \kappa_\delta := \frac{\kappa_s}{\delta}\,, \tag{2.17}$$

where κ_s denotes a new material property and δ is the width of the initial damage.

3. Topological derivative method

In order to complete the underlying steps of the evolving hybrid algorithm, it remains to build-up a method for solving the optimization problem (2.16). Such a task is accomplished herein within the framework of the topological derivative method [31].

The topological derivative is defined as the first term (correction) of the asymptotic expansion of a given shape functional with respect to a small parameter related to the size of singular domain perturbations, such as holes, inclusions and cracks [32]. The well-established framework, built-up on the topological derivative concept, exhibits high potential to be naturally explored in the current context as a steepest-descent direction in the optimization process, likewise any method based on the gradient of a cost functional. In this context, the topological derivative method has been successfully applied in many different areas, such as shape and topology optimization, inverse problems, image processing, multi-scale material design and mechanical modeling including damage and fracture evolution phenomena [33].

We proceed herein within the same context of exploring the topological derivative method to minimize the Francfort-Marigo shape functional (2.7) with respect to the nucleation of a small damaged inclusion, which can occur anywhere in the domain during the crack nucleation/propagation process. Within the hybrid-evolving scheme further discussed herein, under a frozen pore pressure field, the topological derivative associated with elastic subsystem derived in [42], under stationary flow, can be explored in a straightforward fashion to the current transient scenario, as stated in the following result:

Theorem 1. *The topological derivative of the shape functional defined in* (2.7)*, with respect to the nucleation of a small circular inclusion with different mechanical properties from the background, is given by the sum*

$$D_T\mathcal{F}_\omega(x) = D_T\mathcal{J}(x) + \kappa_\delta D_T|\omega|(x), \quad \forall x \in \Omega\,, \tag{3.1}$$

with $D_T|\omega|(x)$ given by

$$D_T|\omega|(x) = \begin{cases} +1, & \text{if } x \in \Omega\backslash\overline{\omega}, \\ -1, & \text{if } x \in \omega, \end{cases} \tag{3.2}$$

and $D_T\mathcal{J}(x)$ represented in the form

$$D_T\mathcal{J}(x) = \mathbb{P}_\gamma\sigma(u)\cdot\varepsilon(u)(x) + (1-\gamma_\alpha)\frac{1+a}{1+a\gamma}\alpha p\mathrm{div}(u)(x) - \frac{(1-\gamma_\alpha)^2}{2\rho\mu(1+a\gamma)}\alpha^2p^2(x)\,, \tag{3.3}$$

where $\mathbb{P}_\gamma$ is the polarization tensor, namely

$$\mathbb{P}_\gamma = -\frac{1}{2}\frac{1-\gamma}{1+b\gamma}\left((1+b)\mathbb{I} + \frac{1}{2}(a-b)\frac{1-\gamma}{1+a\gamma}\mathrm{I}\otimes\mathrm{I}\right)\,, \tag{3.4}$$

with the coefficients a and b defined as

$$a = \frac{\lambda+\mu}{\mu} \quad \text{and} \quad b = \frac{\lambda+3\mu}{\lambda+\mu}\,, \tag{3.5}$$

with the pair $\{\mu,\lambda\}$ given by (2.4)*. Finally, the parameters γ and γ_α denote the contrasts in ρ and α, respectively.*

Proof. The proof of this result can be found in [42], where the general case in which the permeability is also sensitive to the topological perturbation has been considered. □

Remark 2. *It should be noted that, the same formula* (3.1) *holds true for heterogeneous media, provided the heterogeneity is locally Lipschitz continuous* [19].

The underlying iterative gradient descent-based algorithm follows the original ideas proposed in [40], where a small inclusion is nucleated in the region where the topological derivative is negative which provides the descent direction for the Francfort-Marigo shape functional. Computationally, the algorithm is designed to nucleate inclusions with compatible size to the initial damaged region according to the sign of the topological derivative. In order to introduce this idea, let $D_T\mathcal{F}^*_\omega$ be the minimum value of the associated topological derivative, i.e.,

$$D_T\mathcal{F}^*_\omega := \min_{x\in\omega^*} D_T\mathcal{F}_\omega(x)\,, \tag{3.6}$$

with ω^* used to denote the subset where the topological derivative attains negative values, i.e.,

$$\omega^* := \{x \in \Omega : D_T\mathcal{F}_\omega(x) < 0\}\ . \tag{3.7}$$

From these elements, the inclusion to be nucleated within the region ω^*, denoted by ω^β, is defined as

$$\omega^\beta := \{x \in \omega^* : D_T\mathcal{F}_\omega(x) \leq (1-\beta)D_T\mathcal{F}^*_\omega\}\ , \tag{3.8}$$

where $\beta \in (0,1)$ is chosen in such a way that $|\omega^\beta| \approx \pi\delta^2/4$ with δ used to represent the thickness of the initial damage.

It should be noted that the proposed optimization approach obviates the necessity of postulating empirical damage evolution laws to describe crack propagation, leading to a framework more grounded in fundamental issues.

4. The hybrid splitting scheme

We now proceed by incorporating the minimization step associated with the calculation of the topological derivative in the time evolution splitting scheme. As mentioned previously, we shall restrict our analysis to brittle fractures by invoking the underlying hypothesis of propagation occurring in a much faster time-scale compared to the characteristic time inherent to fluid percolation. Such a time-scale assumption hinges upon the phenomenon associated with cracks in brittle materials which grow with speeds much faster than the Darcy velocity. Whence, we assume crack propagation to be instantaneous, so that the pressure field remains frozen as the crack grows. Based on this hypothesis, the pressure field becomes insensitive to the topological perturbations and consequently only the geomechanical system is modified in the sensitivity analysis procedure, by updating the two-value poroelastic coefficients in the healthy and damaged subregions.

The aforementioned discussion suggests pursuing what we refer to as *an hybrid scheme*, where, in contrast to the fixed stress scheme associated with the predictor step, which strongly relies on a frozen total mean stress in the fluid flow module, the optimization loop, based on the topological derivative, strongly relies on a frozen pore pressure field during crack propagation.

In what follows, we present the hybrid algorithm within the context of the time-stepping method. In the framework of the fixed stress (2.13) and (2.14), we consider the backward Euler method in the following form

$$\int_\Omega \sigma(u^n)\cdot\varepsilon(v) = \int_\Omega \alpha p^n \mathrm{div}(v) - \int_\Omega \sigma_0\cdot\varepsilon(v)\,, \quad \forall v \in \mathcal{V}\,, \tag{4.1}$$

$$\int_\Omega \beta^* p^{n+1} q + \Delta t \int_\Omega k\nabla p^{n+1}\cdot\nabla q = \int_\Omega \beta^* p^n q - \int_\Omega \frac{\alpha}{K}\left(\overline{\sigma}^{n+1,m}_{\mathrm{tot}} - \overline{\sigma}^{n}_{\mathrm{tot}}\right) q\,, \quad \forall q \in \mathcal{Q}\,, \tag{4.2}$$

where Δt is the time step, the index n designates the discrete time and m is associated with the iterations between flow and mechanics. Moreover, within the current time-stepping

scheme, the pressure prescribed on Γ_ω is increased by adopting N uniform increments according to (2.15).

Hence, by highlighting the time-scale assumption of the forward poroelastic problem, the total mean stress remains frozen during the iterations performed in the pressure equation until the following convergence criterion is fulfilled,

$$\frac{|\overline{\sigma}_{\text{tot}}^{n+1,m+1} - \overline{\sigma}_{\text{tot}}^{n+1,m}|^2}{|\overline{\sigma}_{\text{tot}}^{n+1,m}|^2} < \text{tol}\,, \tag{4.3}$$

with tol used to denote a prescribed numerical tolerance. Once the fixed-stress iterative scheme has converged, the topological derivative field is evaluated in order to verify whether crack propagation phenomenon will be triggered or not. More precisely, crack propagation will only be activated if the region of negative topological derivative ω^* satisfies $|\omega^*| \geq \pi\delta^2$. Such a methodology avoids the need of introducing another unknown to the system, as commonly adopted in phase-field type models. In Figure 2 we depict the steps of the proposed hybrid scheme, which are further detailed in the form of a pseudo-code described by Algorithm 1.

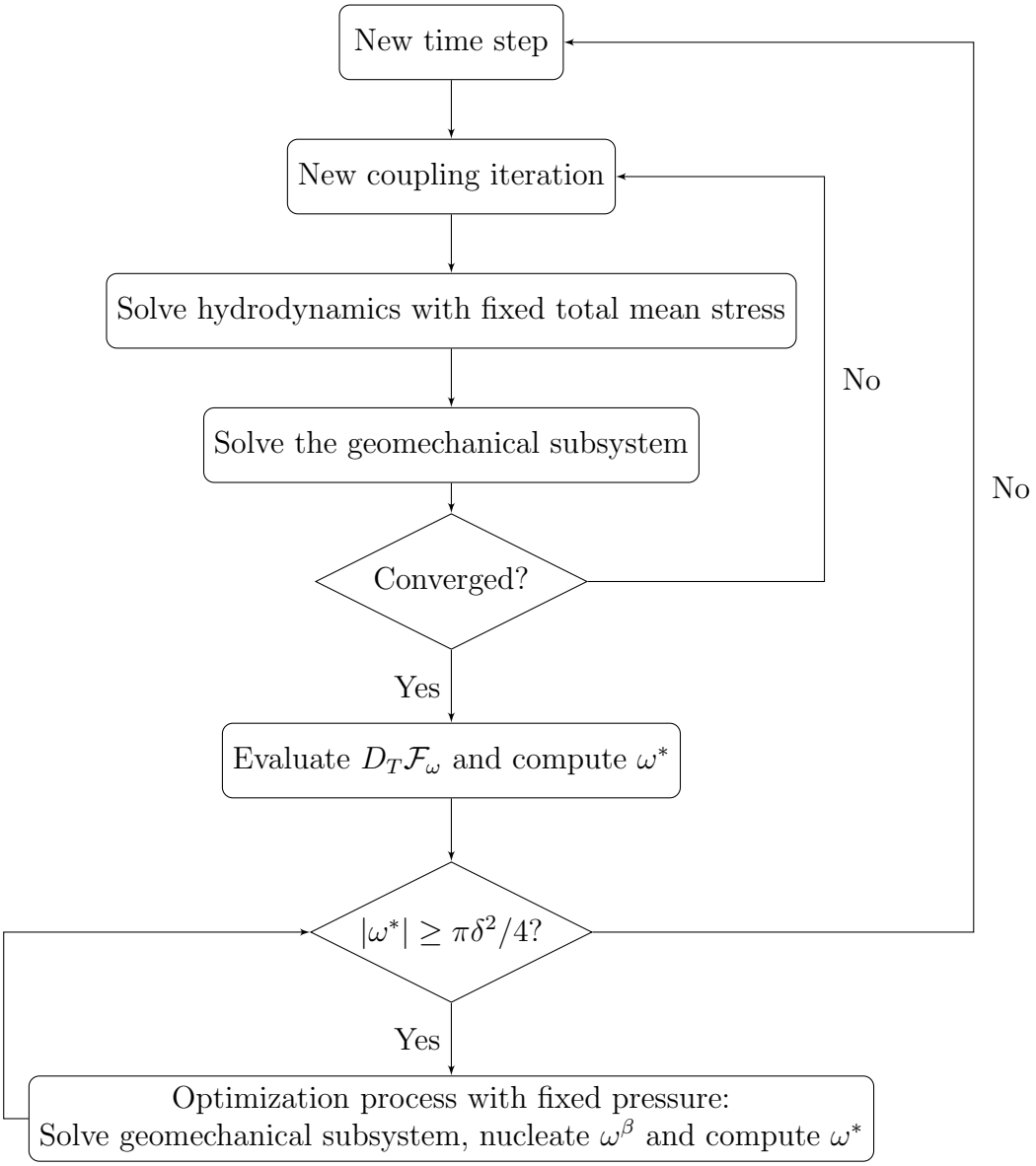

FIGURE 2. Sketch of the steps of the Hybrid scheme.

Algorithm 1: Damage evolution algorithm.

Input : Ω, ω, δ, N, $\overline{p}_0$, r
Output: Optimal topology $\omega^\star$

for $i = 1 : N$ **do**
  increment the time and the prescribed pressure on Γ_ω according to (2.15);
  solve problems (2.14) and (2.13) with fixed stress split scheme;
  evaluate $D_T\mathcal{F}_\omega$ according to (3.1);
  compute the threshold ω^* from (3.7);
  while $|\omega^*| \geq \pi\delta^2/4$ **do**
    intensify the mesh at the crack tip;
    solve the elasticity system (2.13);
    evaluate the topological derivative $D_T\mathcal{F}_\omega$;
    compute the threshold ω^* from (3.7);
    compute the threshold ω^β from (3.8);
    nucleate a new inclusion ω^β inside ω^*;
    update the damaged region: $\omega \leftarrow \omega \cup \omega^\beta$;
    solve the elasticity system and evaluate $D_T\mathcal{F}_\omega$;
    compute the threshold ω^*;
  end while
end for

As mentioned previously, in contrast to the algorithm proposed in [42] under the quasi-static regime, here the pore pressure field remains frozen during the optimization step associated with crack propagation. Consequently, under our hybrid framework of distinct time-scale assumptions in the fixed stress and optimization steps, it is remarkable to observe that only the elasticity system (2.13) is solved during the latter step in the context of Algorithm 1. When combined with the fixed stress scheme, such an assumption simplifies enormously the complexity underlying the coupling between the two phenomena. More specifically, the splitting between the two stages obviates the necessity of computing explicitly the dependence of the topological derivative on the pore pressure field.

Finally, we remark that, unlike Discrete Fracture Models (DFM), our approach does not treat fractures as $(d-1)$-dimensional quantities which would require an additional reduced pressure equation. Here, the Francfort-Marigo functional is associated with the full d-dimensional damage theory rather than fracture in the strict sense. Consequently fracture nucleation and propagation are computed as localized heterogeneities dictated by the topological derivative.

5. Numerical experiments

We shall henceforth illustrate the application of the new numerical modeling in the simulation of propagation of brittle fractures in poroelastic media. For the sake of simplicity, we consider numerical examples in two spatial dimensions, where the reference domain Ω is identified with a $(5 \times 5)\text{m}^2$ square aiming at mimicking a single geological block of the reservoir under plane strain conditions. Such a selected region of analysis contains preexisting fractures represented by an initial nucleated damage region characterized by length h and width δ, along with their hydromechanical properties. We remark that, due to the presence of the infilling material (proppant), the input permeability of the damage zone is not ruled by the cubic law of parallel plates but rather dictated by the infill property [10, 42]. The total time interval $(0, T)$ of gradual pore pressure increase is divided

into N uniform increments. In the simulations we adopt $T = 24$ hours, $N = 200$ and an increment pressure rate $r = 2/3$ MPa/h and $t^* = 12$ hours in (2.15). In all simulation, the convergence of the fixed-stress split was rapidly reached, taking around 2 to 4 iterations to fulfill condition (4.3). Without loss of generality, we neglect the effects of the reference pressure by setting $\overline{p}_0 = 0$, so that the distribution of the *in situ* effective stress balances the overburden. Moreover, in order to compute the *in situ* stress profile in a pre-processing step, we consider the geological block subjected to a vertical stress σ_v applied on the upper boundary Γ_t (see Figure 1) along with oedometric conditions imposed by horizontal displacement constraint on the lateral interfaces Γ_l and Γ_r. Recalling our plane strain assumption, a horizontal stress σ_h is induced with magnitude depending on the Poisson ratio. We remark that the nature of the *in-situ* stress profile, locally dictated by the pair $\{\sigma_v, \sigma_h\}$, plays an essential role in the direction of fracture propagation.

In the notation that follows the subscripts $(\cdot)_m$ and $(\cdot)_f$ are adopted to identify properties in matrix and fracture, respectively. The tolerance for the coupling iterations is set as $\text{tol} = 1 \times 10^{-6}$. The parameter ℓ is introduced to represent the diameter of the inclusion to be nucleated ω^β, which has been assigned heuristically as $\ell = (2/3)\delta$ in order to fulfill the condition $|\omega^\beta| \approx \pi\delta^2/4$.

The spatial discretization associated with the parabolic and elasticity subsystems, (4.1) and (4.2), is performed using the standard Galerkin method adopting linear triangular finite elements.

5.1. **Canonical example.** In this first example, a vertical joint is located in the middle of the lower interface, adjacent to the injection well, as shown in Figure 3. The input data is displayed in Table 1.

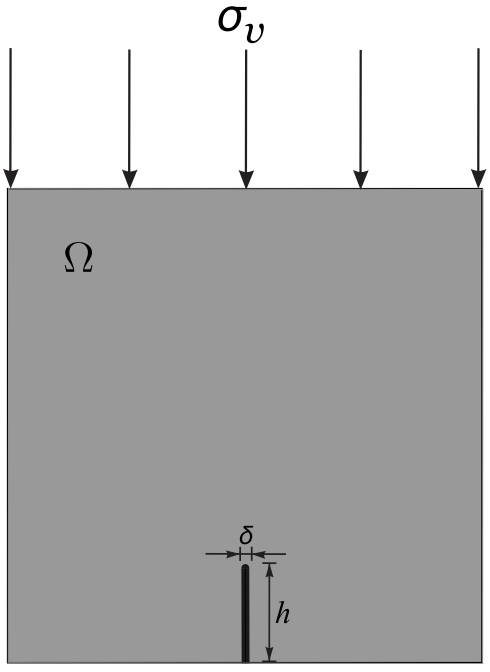

FIGURE 3. Canonical example: One block of the reservoir containing a single geological fracture.

As quoted before, we adopt the same strategy of [41, 42] in order to quantify the critical pressure of crack activation p_c. Such a scalar represents the pore pressure values in which the first inclusion is nucleated. In this setting, we perform numerical experiments with different input values of the width δ associated with the initial damage

$$\delta \in \{1/20,\ 1/40,\ 1/80,\ 1/160,\ 1/320\}\text{m}\ . \tag{5.1}$$

TABLE 1. Canonical example: Parameters.

Parameter	Value	Parameter	Value
h	1.0 m	E	30 GPa
δ	Eq. (5.1)	ρ_0	10^{-4}
$\overline{p}_0$	0 MPa	ν	0.3
$\overline{p}^*$	4 MPa	K_m	25 GPa
t^*	12 h	K_f	2.5 MPa
κ_s	60.0 J/m	β_m^*	0.037 GPa^{-1}
σ_v	3.5 MPa	β_f^*	0.40 MPa^{-1}
α_m	0.75	k_m	15 mD
α_f	1.0	k_f	15 D

The critical pressures obtained from the tests are then normalized with respect to the first value of the sequence p_c^0 associated with $\delta = 1/20$m, as illustrated in Figure 4. Furthermore, the introduction of parameter κ_δ from (2.17) allows to cope with reliable values of the critical pressure (blue dashed line). On the other hand, in the absence of such correction factor, the critical pressure decreases as the width δ becomes smaller (red dashed line). We also remark that the result reported in Figure 4 can be envisioned as a numerical evidence of the Γ-convergence of the proposed damage approach to a hydraulic fracture model [9].

A well-known limitation of approaches based on the Francfort-Marigo damage model is the fact that it is not able to distinguish between traction and compression states. In this sense, in order to avoid crack propagation under compressive stress, we have adopted the heuristic numerical scheme proposed in [40]. The basic idea consists in checking whether the trace of the stress tensor is positive, namely $\mathrm{tr}(\sigma(u(x))) > 0$, to allow for crack growth.

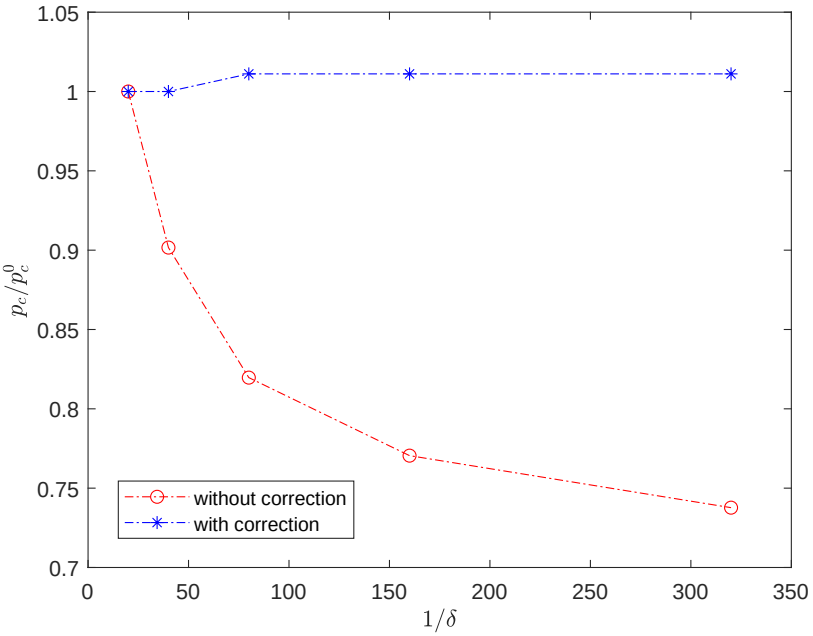

FIGURE 4. Canonical example: Convergence test for the critical pressure.

The ability of the model in successfully characterize the critical pressure allows to perform reliable numerical simulations. In fact, by setting $\delta = 1/40$m, the first computed

critical pressure $p_c^0 = 3.44$ MPa suggests fracture activation at $t = 5.5$ hours, which ratifies the necessity of incorporating transient effects in the fixed-stress split formulation. Figure 5(a) illustrate the crack tip in the finite element mesh whereas Figure 5(b) displays the topological derivative field immediately before the first propagation. Moreover, in the evolution process, the following subsequent values of the critical pressures are computed, $p_c^0 = 3.60$ MPa, $p_c^1 = 3.64$ MPa, $p_c^2 = 3.68$ MPa, $p_c^3 = 3.72$ MPa and $p_c^5 = 3.76$ MPa. Finally, in Figure 6 we display the scenario of initial damage along with the subsequent path of propagation obtained with the corrected approach. As expected, adopting the correction procedure, we observe a straight crack path which is typical of the problem setting. The final mesh used to discretize the domain Ω has 755250 elements and a total of 255 iterations were performed in the optimization process.

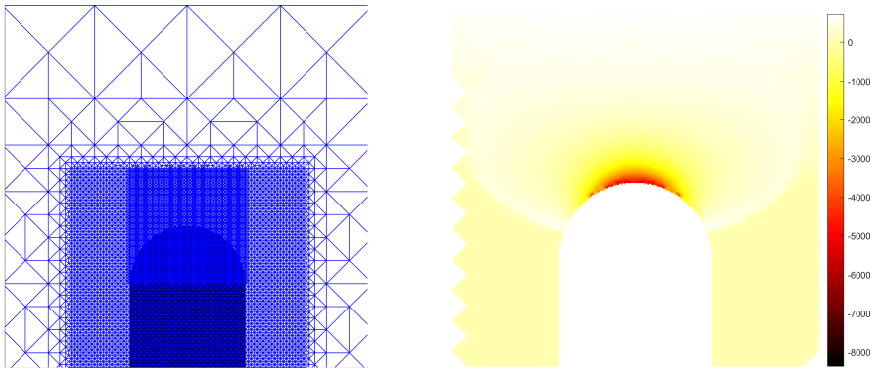

(a) finite element mesh (b) topological derivative field

FIGURE 5. Representation of the finite element mesh and topological derivative field at the crack tip.

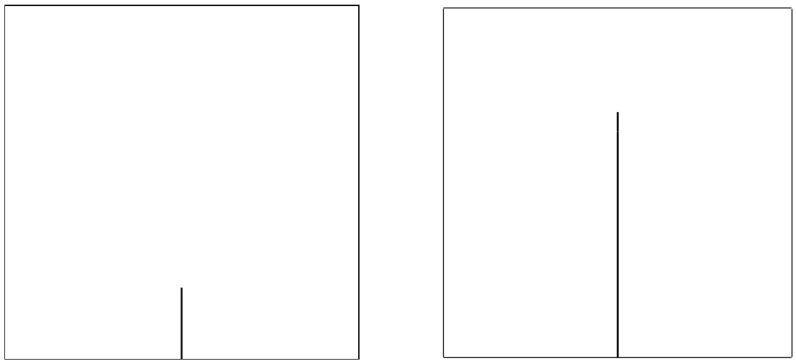

(a) initial fracture (b) final fracture

FIGURE 6. Canonical example: Damage evolution.

5.2. **Effects of rock heterogeneity.** We consider the same geometry and boundary conditions of the previous example with both permeability k and Young modulus E fields corrupted by an uncorrelated White Gaussian Noise (WGN) perturbation of zero mean and standard deviation τ. The corresponding parametrizations read as $k_\tau = k(1 - \tau_p s)$ and $E_\tau = E(1 + \tau_e s)$, with $s : \Omega \to \mathbb{R}$ a function assuming random values in the interval $(0, 1)$ and $\tau_p = 0.5$ and $\tau_e = 2.0$ the related noise levels. In Figure 7 we depict a single realization of the random fields. Input parameters are presented in Table 2. The damage evolution associated with each critical pressure is presented in Figure 8. We remark that

the effects of matrix heterogeneity manifest in the appearance of phenomena such as kinking and bifurcations stemming from perturbation in the hydromechanical properties. The final mesh used to discretize the domain Ω has 1008122 elements and a total of 156 iterations were performed in the optimization process.

TABLE 2. Heterogeneous medium: Parameters.

Parameter	Value	Parameter	Value
h	1.0 m	E	17 GPa
δ	0.0625 m	ρ_0	10^{-4}
$\overline{p}_0$	0 MPa	ν	0.3
$\overline{p}^*$	4 MPa	K_m	9.45 GPa
t^*	12 h	K_f	0.945 MPa
κ_s	150.0 J/m	β_m^*	0.12 GPa^{-1}
σ_v	3.5 MPa	β_f^*	0.60 MPa^{-1}
α_m	0.75	k_m	40 mD
α_f	1.0	k_f	40 D

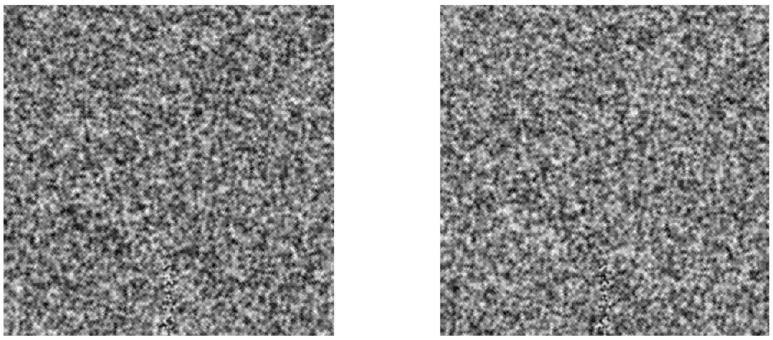

(a) corrupted Young modulus (b) corrupted permeability

FIGURE 7. Heterogeneous medium: Corrupted properties.

5.3. **Effects of stratification.** We now analyze the effects of a depositional environment upon the crack path by considering the geological block composed of two layers with different Young modulus and a single permeability, namely $E_1 = 17$ GPa and $E_2 = 2E_1$. Input parameters are summarized in Table 3. The two scenarios treated in this example are depicted in Figure 9. In the first one, designated by Case 1, the fracture propagates towards the stiffer layer. In this setting, six distinct critical pressures have been detected. The first one observed at $t = 5$ h ($p_c^0 = 3.36$ MPa) and the last at $t = 6$ h ($p_c^5 = 3.90$ MPa). We may observe propagation occurring initially in the vertical direction tending to align with the interface with the proximity of the stiffer layer, as shown in Figure 10(a). In the second scenario, denoted as Case 2, fracture propagates towards the more soft layer. Again, different critical pressures were observed, with $p_c^0 = 4.88$ MPa at $t = 7.3$ h and $p_c^3 = 5.20$ MPa at $t = 8$ h. In this setting the fracture tends to propagate in the vertical direction but with a slight deviation to the right, after crossing the interface between the layers, as shown in Figure 10(b). The final mesh used to discretize the domain Ω has 539008 elements in Case 1 and 526680 in Case 2 and a total of 180 iterations were performed in the optimization process in both cases.

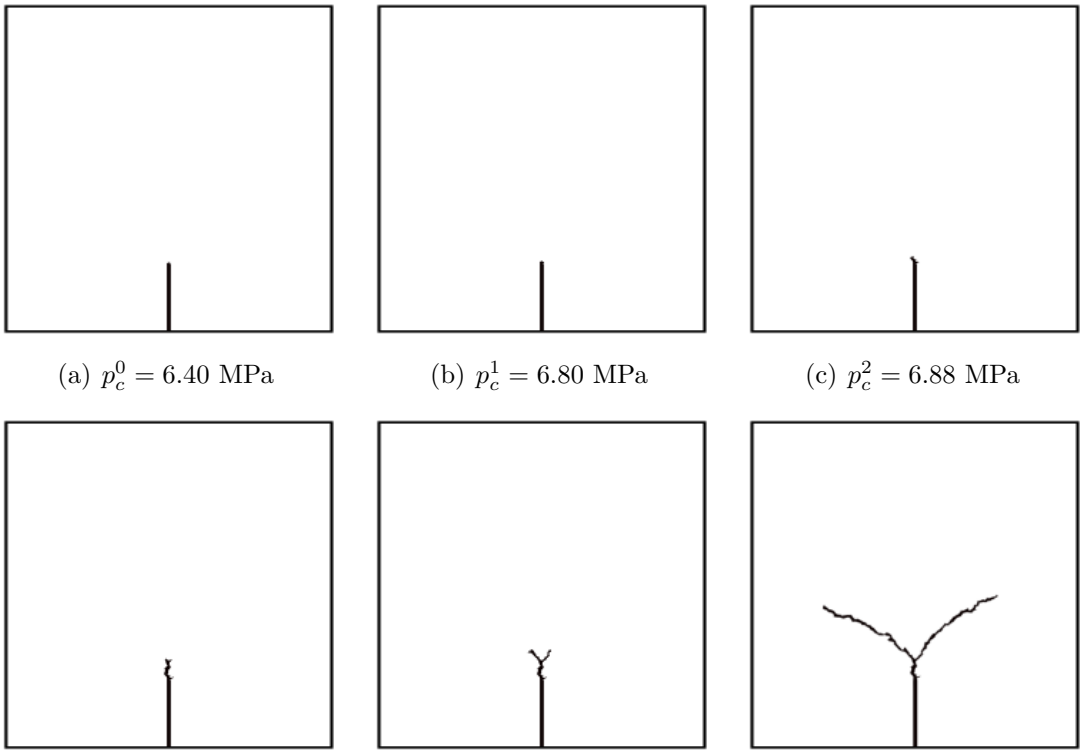

(a) $p_c^0 = 6.40$ MPa (b) $p_c^1 = 6.80$ MPa (c) $p_c^2 = 6.88$ MPa

(d) $p_c^3 = 6.96$ MPa (e) $p_c^4 = 7.04$ MPa (f) $p_c^5 = 7.12$ MPa

FIGURE 8. Heterogeneous medium: Damage evolution.

TABLE 3. Stratified block: Parameters.

Parameter	Value	Parameter	Value
h	1.0 m	E_1	17 GPa
δ	0.0625 m	ρ_0	10^{-4}
$\overline{p}_0$	0 MPa	ν	0.3
$\overline{p}^*$	4 MPa	K_m	9.45 GPa
t^*	12 h	K_f	0.945 MPa
κ_s	20.0 J/m	β_m^*	0.12 GPa^{-1}
σ_v	3.5 MPa	β_f^*	0.60 MPa^{-1}
α_m	0.75	k_m	40 mD
α_f	1.0	k_f	40 D

5.4. **Effects of stratification and heterogeneity.** Likewise the previous example, we now analyze the effects of the depositional environment by considering the geological block composed of two layers with different Young modulus and permeabilities, namely $E_1 = 17$ GPa and $E_2 = 2E_1$ and $k_1 = 40$ mD and $k_2 = k_1/2$. Such properties are also corrupted by a WGN of zero mean and standard deviation τ, according to the previous example. We consider two distinct scenarios differing from each other by the spatial distribution of the material properties as shown in Figure 11. In the scenario denoted by Case 1, five distinct critical pressures were detected, particularly $p_c^0 = 4.72$ MPa at $t = 7$ h and $p_c^4 = 5.72$ MPa at $t = 8.5$ h. In addition to the presence of kinking and bifurcations reported in the previous example, we also observe a trend in propagation towards the common interface. On the other hand, a combination of *in situ* stress and heterogeneity also leads to the counter-intuitive propagation across the more rigid layer. In a similar fashion, in Case 2

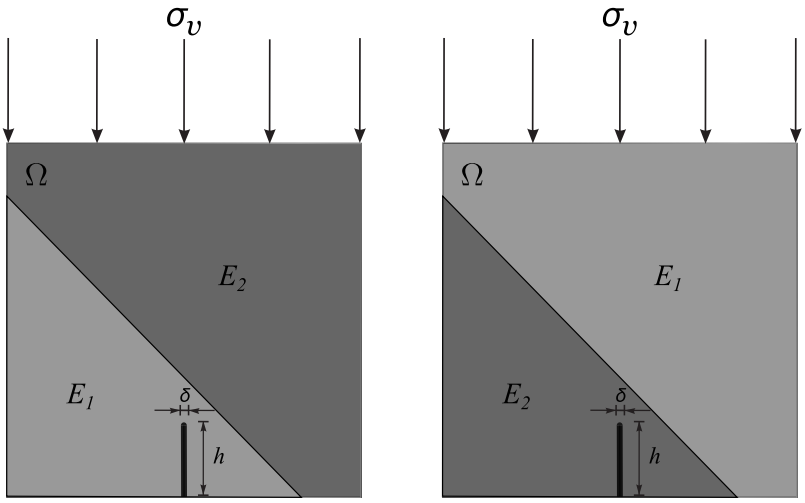

(a) Case 1 (b) Case 2

FIGURE 9. Stratified block: Material distribution.

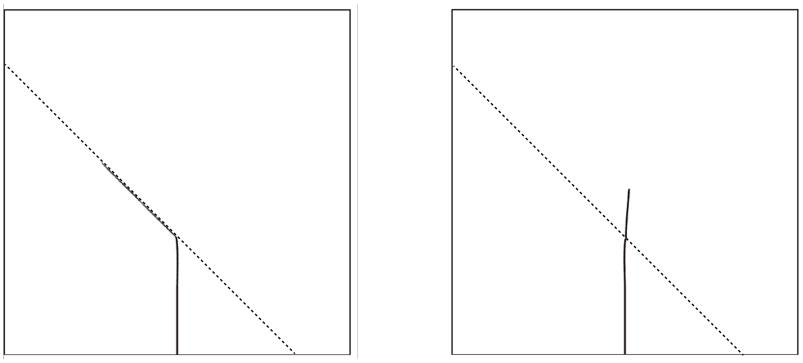

(a) Case 1 (b) Case 2

FIGURE 10. Stratified block: Final results.

we also observe kinks and bifurcations and propagation in both layers as shown in Figure 12. The final mesh used to discretize the domain Ω has 823810 elements in Case 1 and 929094 in Case 2 and a total of 150 iterations were performed in the optimization process in both cases.

5.5. **Effects of the Poisson ratio.** In the subsequent numerical experiments, we aim at analyzing the influence of the Poisson ratio upon the orientation of crack growth. To this end, we have adapted the example discussed in [12, 42] to a scenario in which the magnitude of the horizontal stress σ_h is directly computed from the pair $\{\sigma_v, \nu\}$, under the lateral displacement constraint which furnishes $\sigma_h = \sigma_v\,\nu/(1-\nu)$, under the plane strain assumption. The preexisting crack is located at the center of the interface forming an angle of 30° with respect to the horizontal axis (Figure 13). The input data used in the simulation is summarized in Table 4. In this setting, we perform simulations with different values of the Poisson's ratio $\nu \in \{0.1, 0.2, 0.3, 0.4\}$, which furnished a single critical pressure $p_c^0 = 1.08$ MPa at $t = 1.5$ h (see Figure 14). In all cases the final mesh used to discretize the domain Ω has approximately 400000 elements and a total of 80 iterations were performed in the optimization process.

5.6. **Interaction between multiple fractures.** In this example, we consider the same geological block containing three preexisting cracks. Two lie within the block whereas the

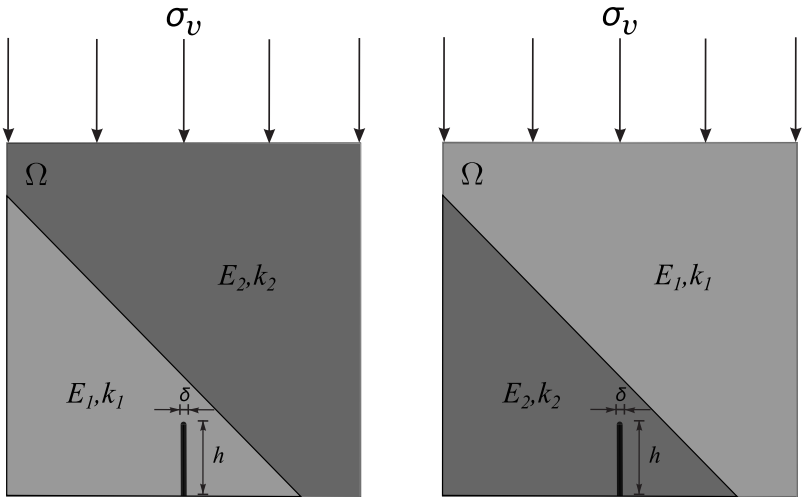

(a) Case 1 (b) Case 2

FIGURE 11. Stratified and heterogeneous block: Material distribution.

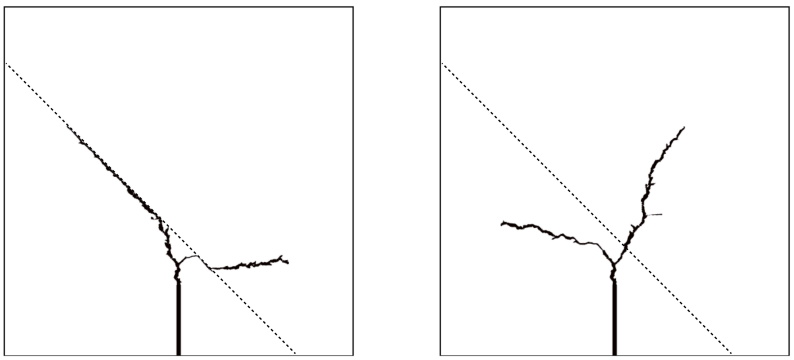

(a) Case 1 (b) Case 2

FIGURE 12. Stratified and heterogeneous block: Crack configuration after propagation.

TABLE 4. Poisson ratio effect: Parameters.

Parameter	Value	Parameter	Value
h	1.0 m	E	10 GPa
δ	0.0625 m	ρ_0	10^{-5}
$\overline{p}_0$	0 MPa	ν	0.3
$\overline{p}^*$	8 MPa	K_m	8.4 GPa
t^*	12 h	K_f	0.084 MPa
κ_s	1.85×10^5 J/m	β_m^*	0.01 GPa^{-1}
σ_v	3.5 MPa	β_f^*	1.03 MPa^{-1}
α_m	0.1	k_m	40 mD
α_f	1.0	k_f	40 D

third crack is located at the pressurized wellbore, as shown in Figure 15. In this scenario, our aim is to highlight the complex task of determining the crack path under simultaneous influence of the prescribed *in situ* stress state and mutual interactions between evolving fractures. Input parameters used are presented in Table 5. The proposed framework was capable of detecting fifteen distinct critical pressures. In particular we computed the

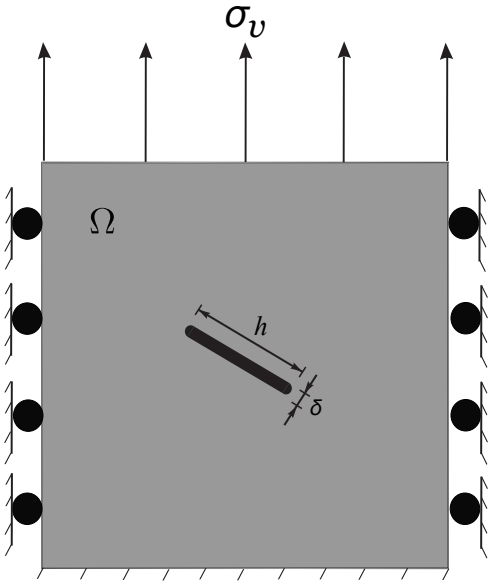

FIGURE 13. Selected example of a geological block subject to lateral constraints and an prescribed overburden on the top boundary

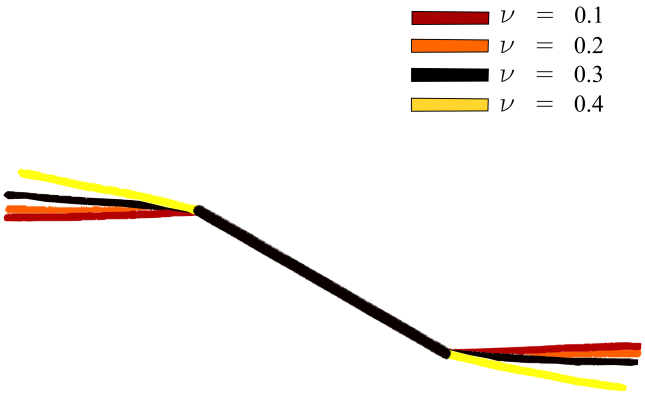

FIGURE 14. Study of the influence of the Poisson ratio on crack pattern: Zoom of the damage zone after propagation.

activation pressure value $p_c^0 = 4.24$ MPa along with the last critical pressure $p_c^{14} = 5.40$ MPa. Finally, in Figure 16, we display the initial fracture locations along with the final configuration after propagation. The final mesh used to discretize the domain Ω has 1555667 elements and a total of 246 iterations were performed in the optimization process.

5.7. **Influence of the *in situ* stress.** Finally, in our last set of simulations we consider the example discussed in [44], of three preexisting horizontal cracks separated by a distance d, as depicted in Figure 17. Unlike the previous cases, the injection well is located at the left boundary of the block where the gradual pressure increase ruled by (2.15) is enforced. In contrast with the previous examples, homogeneous Dirichlet boundary conditions are prescribed on the other three boundaries. Two combinations of *in situ* stresses are considered. In the first scenario we set $\sigma_h = 2.0$ MPa and $\sigma_v = 1.0$ MPa, whereas in the second $\sigma_h = 1.0$ MPa and $\sigma_v = 2.0$ MPa. Following [44], our aim here consists in computing the sensitivity of the hydraulic fracture pattern with the profile of the *in situ* stress. Input parameters are presented in Table 6. In the first scenario, only one critical pressure $p_c^0 = 4.16$ MPa was observed. As expected, the central crack

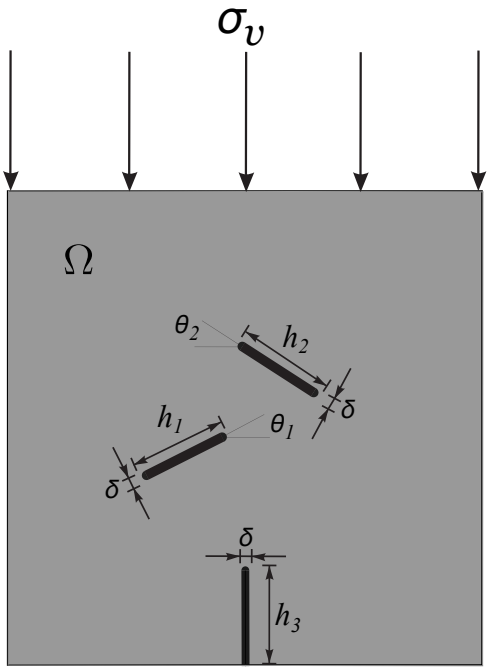

FIGURE 15. Geological block containing three fractures before propagation.

TABLE 5. Multiple fractures: Parameters.

Parameter	Value	Parameter	Value
h_1	1.0 m	θ_1	$\pi/8$ rad
h_2	1.0 m	θ_2	$\pi/6$ rad
h_3	1.25 m	E	17 GPa
δ	0.0625 m	ρ_0	10^{-4}
$\overline{p}_0$	0 MPa	ν	0.2
$\overline{p}^*$	8 MPa	K_m	9.45 GPa
t^*	12 h	K_f	0.945 MPa
κ_s	240.0 J/m	β_m^*	0.12 GPa^{-1}
σ_v	3.5 MPa	β_f^*	0.60 MPa^{-1}
α_m	0.75	k_m	70 mD
α_f	1.0	k_f	70 D

propagates horizontally, while the upper and lower cracks initially deviate from that pattern but with a trend of horizontal reorientation 18(a) (Case 1)). In contrast, in the second scenario, two distinct critical pressures $p_c^0 = 5.28$ MPa and $p_c^0 = 5.36$ MPa were detected. As expected, the three cracks grow toward the direction of maximum *in situ* stress. Nevertheless, as depicted in Figure 18(b) (Case 2), a non-intuitive pattern in which all three cracks bifurcate is also observed. Finally, for the sake of completeness, considering Case 2 in Figure 19 we show the evolution of the damage with the iterations inherent to the optimization process with a critical pressure $p_c^0 = 5.28$ MPa. The final mesh used to discretize the domain Ω has 1116074 elements in Case 1 and 1586462 in Case 2. A total of 83 iterations were performed in the optimization process for Case 1, while 138 were performed in Case 2.

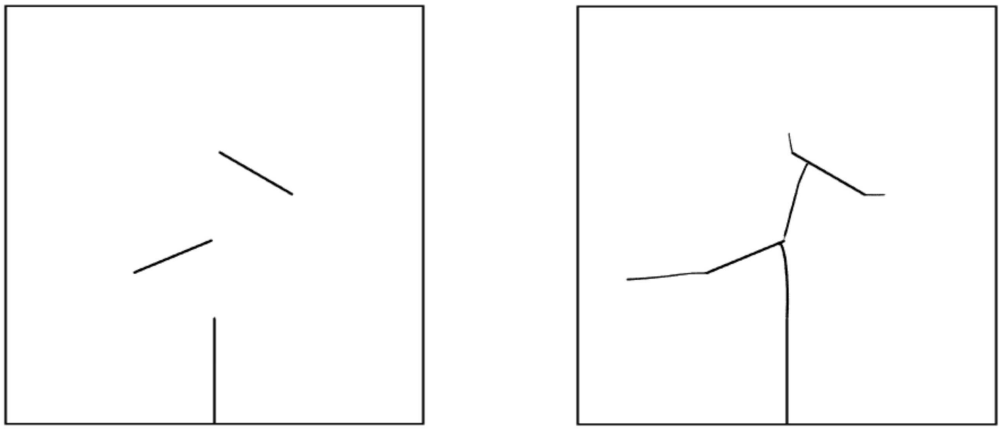

(a) initial fracture configuration (b) final configuration after propagation

FIGURE 16. Damage evolution in a scenario of mutual interacting fractures

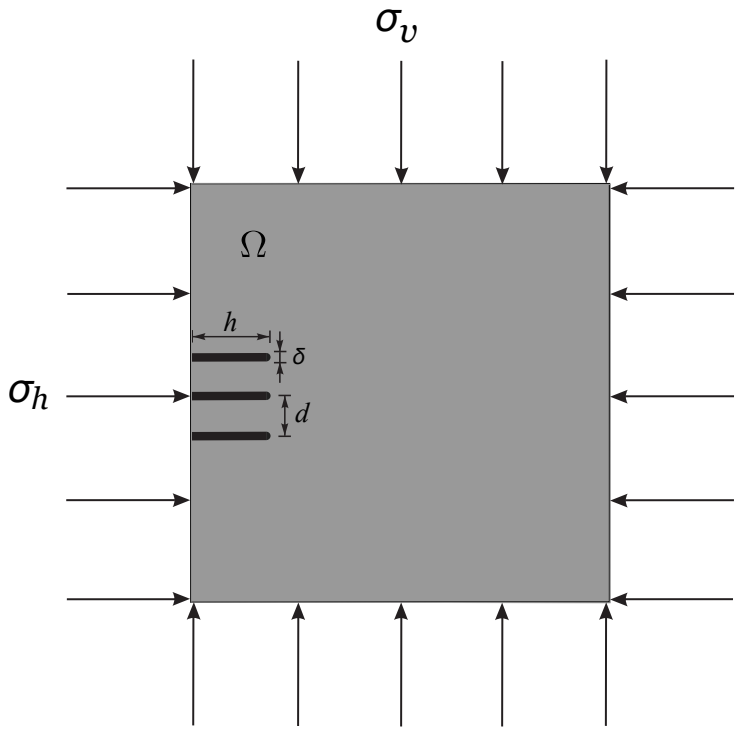

FIGURE 17. Influence of *in situ* stress: Block containing three horizontal cracks.

6. Conclusions

This paper aimed at the extension of the hydro-mechanical model of crack propagation proposed in [42] to the transient regime. Within this framework, we constructed an alternative description of crack propagation in poroelastic media based on a hybrid approach which explored the characteristic time-scales underlying the fixed stress split method for poroelasticity and an optimization methodology relying on the topological derivative concept. Unlike phase-field based-models, which entail regularization and introduce explicitly a parameter in the field-equations, the formulation proposed herein shows the ability to handle the Francfort-Marigo damage functional in its original form, based on the propagation of the abrupt interface between damaged and intact rock matrix.

TABLE 6. Influence of *in situ* stress: Parameters.

Parameter	Value	Parameter	Value
h	1.0 m	E	17 GPa
δ	0.0125 m	ρ_0	10^{-2}
$\overline{p}_0$	0 MPa	ν	0.2
$\overline{p}^*$	8 MPa	K_m	9.45 GPa
t^*	12 h	K_f	94.5 MPa
κ_s	150 J/m	β_m^*	0.07 GPa^{-1}
σ_v	3.5 MPa	β_f^*	0.01 MPa^{-1}
α_m	0.75	k_m	1 mD
α_f	1.0	k_f	1 D

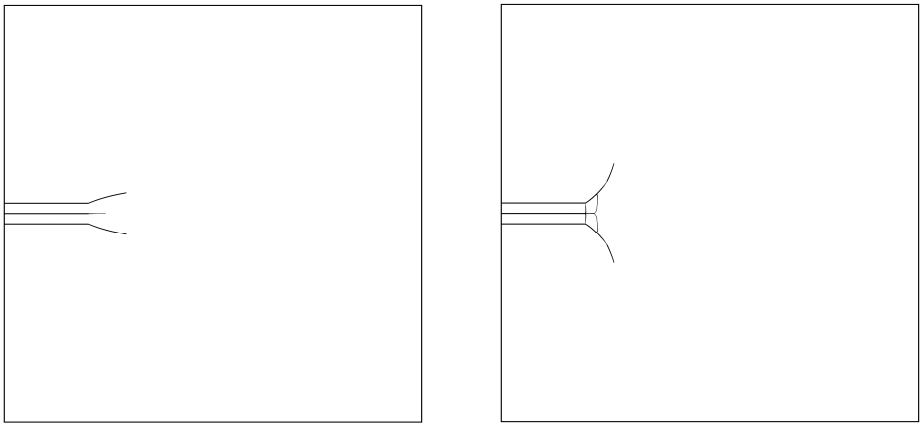

(a) Case 1 (b) Case 2

FIGURE 18. Influence of *in situ* stress upon crack grow.

Implementation of the hybrid approach was performed within a straightforward post-processing approach with the topological derivative envisioned as a gradient descent direction for the Francfort-Marigo functional in the minimization procedure. The proposed approach was capable of preserving the original structure of the equations governing the hydro-mechanical coupling and only updates the poroelastic parameters within the two distinct regions.

In addition, it is worth mentioning the remarkable property underlying Algorithm 1, which consists of a local optimality condition based on the topological derivative that has been fulfilled in all examples. More precisely, the crack path is characterized by the evolution of the negative regions of the topological derivative field. Moreover, for a sufficient refined mesh, as used in the numerical experiments presented in Section 5, any mesh dependence with respect to the localization of these negative regions during the crack advance – and therefore to the crack trajectory – has been observed. On the other hand, owing to its gradient descent nature, it is not possible to ensure global optimality of the outcomes. Nonetheless, the outcome can be envisioned as a local optimum of the Francfort-Marigo shape functional. In spite of this drawback, the method has shown reliability for reproducing existing results and producing acceptable/expected crack paths. Furthermore, the avoidance of the necessity of introducing a regularization parameter, like in phase-field theories, along with the allowance of using traditional Galerkin-type methods (no need for basis enrichment), provides new perspectives for exploring the

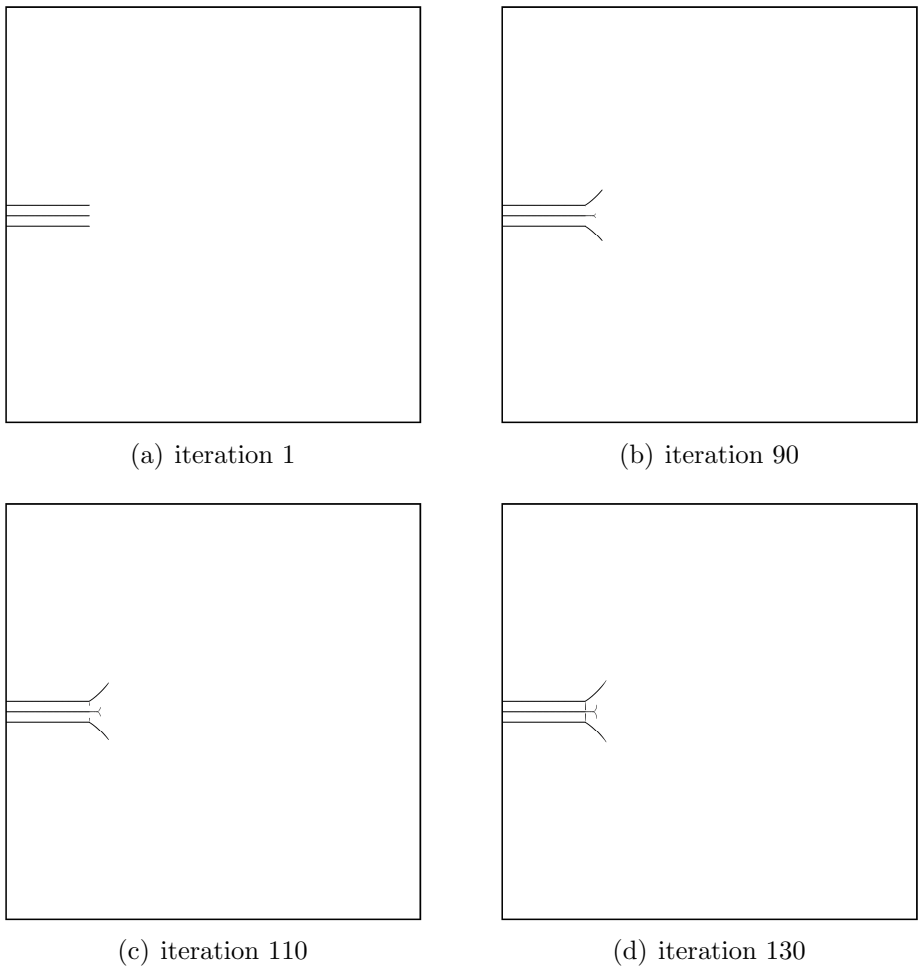

(a) iteration 1 (b) iteration 90

(c) iteration 110 (d) iteration 130

FIGURE 19. Influence of *in situ* stress: Damage path during the optimization process for Case 2 at $p_c^0 = 5.28$ MPa.

framework of the topological derivative in simulating crack propagation in poroelastic media.

Computational simulations, performed in benchmark examples, illustrated the ability of the method to capture important features in hydraulic fracturing such as bifurcation of multiple cracks and characterization of critical pressures. Finally, it is remarkable to see the non-intrusive form of the method wherein the computational of the topological derivative is performed in the previously mentioned simple post-processing approach with poroelastic parameters updated in distinct manners within the two sub-regions. Finally, a stability analysis of the Picard scheme between the topological derivative loop and the geomechanics subsystem of the fixed stress split remains an open issue and will be subject of future work. In addition, the use of a prescribed injection rate rather than Dirichlet-type pressure protocol will be treated in future works as well as the implementation of a robust post-processing approach for evaluation of crack width during propagation.

ACKNOWLEDGEMENTS

This research was partly supported by CNPq (Brazilian Research Council), CAPES (Brazilian Higher Education Staff Training Agency) and FAPERJ (Research Foundation of the State of Rio de Janeiro). These supports are gratefully acknowledged.

References

[1] G. Allaire, F. Jouve, and N. Van Goethem. Damage and fracture evolution in brittle materials by shape optimization methods. *Journal of Computational Physics*, 230(12):5010–5044, 2011.

[2] T. Almani, K. Kumar, A. Dogru, G. Singh, and M.F. Wheeler. Convergence analysis of multirate fixed-stress split iterative schemes for coupling flow with geomechanics. *Computer Methods in Applied Mechanics and Engineering*, 311:180–207, 2016.

[3] L. Ambrosio and V. M. Tortorelli. Approximation of functionals depending on jumps by elliptic functionals via γ-convergence. *Communications on Pure and Applied Mathmatics*, 43(8):999–1036, 1990.

[4] G. I. Barenblatt. Mathematical theory of equilibrium cracks in brittle fracture. *Advances in Applied Mechanics*, 7:55–129, 1962.

[5] M. A. Biot. General theory of three-dimensional consolidation. *Journal of Applied Physics*, 12(2):155–164, 1941.

[6] M. A. Biot and D. Willis. The elastic coefficients of the theory of consolidation. *Journal of Applied Mechanics*, 24:594–601, 1957.

[7] B. Bourdin, G. A. Francfort, and J. J. Marigo. The variational approach to fracture. *Journal of Elasticity*, 91(1-3):5–148, 2008.

[8] T. D. Cao, E. Milanese, E. W. Remij, P. Rizzato, J. J. C. Remmers, L. Simoni, J. M. Huyghe, F. Hussain, and B. A. Schrefler. Interaction between crack tip advancement and fluid flow in fracturing saturated porous media. *Mechanics Research Communications*, 80:24–37, 2017.

[9] M. Caroccia and N. Van Goethem. Damage-driven fracture with low-order potentials: Asymptotic behavior, existence and applications. *ESAIM: Mathematical Modelling and Numerical Analysis*, 53(4):1305–1350, 2019.

[10] B. Carrier and S. Granet. Numerical modeling of hydraulic fracture problem in permeable medium using cohesive zone model. *Enginnering Fracture Mechanics*, 79:312–328, 2012.

[11] A. Cheng. *Poroelasticity*. Springer, 2016.

[12] C. Chukwudozie, B. Bourdin, and K. Yoshioka. A variational approach to the modeling and numerical simulation of hydraulic fracturing under in-situ stresses. *in: Proceedings of the 38th Workshop on Geothermal Reservoir Engineering*, 2013.

[13] C. Chukwudozie, B. Bourdin, and K. Yoshioka. A variational phase-field model for hydraulic fracturing in porous media. *Computer Methods in Applied Mechanics and Engineering*, 347:957–982, 2019.

[14] J. B. Clark. A hydraulic process for increasing the productivity of wells. *Trans Am Inst Mining Metal Eng*, 186(1):1–8, 1949.

[15] R. H. Dean, X. Gai, C. M. Stone, and S. E. Minkoff. A comparison of techniques for coupling porous flow and geomechanics. *SPE Journal*, 11(1):132–140, 2006.

[16] A. Egger, U. Pillai, K. Agathos, E. Kakouris, E. Chatzi, I. A. Aschroft, and S. P. Triantafyllou. Discrete and phase field methods for linear elastic fracture mechanics: A comparative study and state-of-the-art review. *Applied Sciences*, 9(12), 2019.

[17] G. Francfort and J. J. Marigo. Revisiting brittle fracture as an energy minimization problem. *Journal of the Mechanics and Physics of Solids*, 46(8):1319–1342, 1998.

[18] G. A. Francfort and J. J. Marigo. Stable damage evolution in a brittle continuous medium. *European Journal of Mechanics, A/Solids*, 12(2):149–189, 1993.

[19] S. M. Giusti, A. Ferrer, and J. Oliver. Topological sensitivity analysis in heterogeneous anisotropic elasticity problem. Theoretical and computational aspects. *Computer Methods in Applied Mechanics and Engineering*, 311:134–150, 2016.

[20] J. Kim and G. J. Moridis. Stability, accuracy and efficiency of sequential methods for coupled flow and geomechanics. *SPE Reservoir simulation symposium*, 2011.

[21] J. Kim and G. J. Moridis. Numerical analysis of fracture propagation during hydraulic fracturing operations in shale gas systems. *International Journal of Rock Mechanics & Mining Sciences*, 76:127–137, 2015.

[22] J. Kim, H. A. Tchelepi, and R. Juanes. Stability and convergence of sequential methods for coupled flow and geomechanics: Fixed-stress and fixed-strain splits. *Computer Methods in Applied Mechanics and Engineering*, 200:1591–1606, 2011.

[23] S. Lee, A. Mikelić, M. F. Wheeler, and T. Wick. Phase-field modeling of two phase fluid filled fractures in a poroelastic medium. *SIAM Multiscale Modeling and Simulation*, 16(4):1542–1580, 2018.

[24] R. W. Lewis and B. A. Schrefler. *The finite element method in the deformation and consolidation porous media*. Wiley, 1987.

[25] A. Mikelić and M. F. Wheeler. Convergence of iterative coupling for coupled flow geomechanics. *Computational Geosciences*, 17(3):455–461, 2013.
[26] N. Moes, J. Dolbow, and T. Belytschko. A finite element method for crack growth without remeshing. *International Journal for Numerical Methods in Engineering*, 46:131–150, 1999.
[27] D. Mumford and J. Shah. Optimal approximations by piecewise smooth functions and associated variational problems. *Communications on Pure and Applied Mathematics*, 42(5):577–685, 1989.
[28] M. A. Murad and A. F. D. Loula. Improved accuracy in finite element analysis of Biot's consolidation problem. *Computer Methods in Applied Mechanics and Engineering*, 95(3):359–382, 1992.
[29] M. A. Murad and A. F. D. Loula. On stability and convergence of finite element approximations of Biot's consolidation problem. *International Journal for Numerical Methods in Engineering*, 37:645–667, 1994.
[30] M. A. Murad, V. Thomée, and A. F. D. Loula. Asymptotic behavior of semidiscrete finite-element approximations of Biot's consolidation problem. *SIAM Journal on Numerical Analysis*, 33(3):1065–1083, 1996.
[31] A. A. Novotny and J. Sokołowski. *Topological derivatives in shape optimization*. Interaction of Mechanics and Mathematics. Springer-Verlag, Berlin, Heidelberg, 2013.
[32] A. A. Novotny and J. Sokołowski. *An introduction to the topological derivative method*. Springer Briefs in Mathematics. Springer Nature Switzerland, 2020.
[33] A. A. Novotny, J. Sokołowski, and A. Żochowski. *Applications of the topological derivative method*. Studies in Systems, Decision and Control. Springer Nature Switzerland, 2019.
[34] P. J. Phillips and M. F. Wheeler. Overcoming the problem of locking in linear elasticity and poroelasticity: an heuristic approach. *Computational Geosciences*, 13(1):5–12, 2008.
[35] S. Salimzadeh, A. Paluszny, and R. W. Zimmerman. Three-dimensional poroelastic effects during hydraulic fracturing in permeable rocks. *International Journal of Solids and Structures*, 108:153–163, 2017.
[36] P. Samier, A. Onaisi, and S. Gennaro. A practical iterative scheme for coupling geomechanics with reservoir simulation. *SPE Reservoir & Evaluation Engineering*, 11, 2008.
[37] S. Secchi and B. A. Schrefler. A method for 3-d hydraulic fracturing simulation. *International Journal of Fracture*, 178(1):245–258, 2012.
[38] D. Tran, A. Settari, and L. Nghiem. New iterative coupling between a reservoir simulator and a geomechanics module. *SPE Journal*, 9(03):362–369, 2004.
[39] N. Van Goethem and A. A. Novotny. Crack nucleation sensitivity analysis. *Mathematical Methods in the Applied Sciences*, 33(16):1978–1994, 2010.
[40] M. Xavier, E. A. Fancello, J. M. C. Farias, N. Van Goethem, and A. A. Novotny. Topological derivative-based fracture modelling in brittle materials: A phenomenological approach. *Engineering Fracture Mechanics*, 179:13–27, 2017.
[41] M. Xavier, A. A. Novotny, and N. Van Goethem. A simplified model of fracking based on the topological derivative concept. *International Journal of Solids and Structures*, 139–140:211–223, 2018.
[42] M. Xavier, N. Van Goethem, and A. A. Novotny. Hydro-mechanical fracture modeling governed by the topological derivative method. *Computer Methods in Applied Mechanics and Engineering*, 365:112974, 2020.
[43] G. Q. Zhang and M. Chen. Dynamic fracture propagation in hydraulic re-fracturing. *Journal of Petroleum Science and Engineering*, 70:266–272, 2010.
[44] S. Zhou and J. Ma. Phase field characteristic multizone hydraulic fracturing in porous media: the effect of stress boundary. *European Journal of Environmental and Civil Engineering*, pages 1–21, 2020.

(J.M.M. Luz Filho, M.A. Murad, A.A. Novotny) Laboratório Nacional de Computação Científica LNCC/MCTI, Coordenação de Métodos Matemáticos e Computacionais, Av. Getúlio Vargas 333, 25651-075 Petrópolis - RJ, Brasil

Email address: {jmorvan,murad,novotny}@lncc.br

(M. Xavier) Universidade Federal Fluminense UFF, Departamento de Engenharia Mecânica, Rua Passo da Pátria 156, 24210-240 Niterói - RJ, Brasil

Email address: marcelxavier@id.uff.br